Importance of resonance widths in low-energy scattering of weakly bound light-mass nuclei

P. R. Fraser,[1,*] K. Massen-Hane,[1] K. Amos,[2,3] I. Bray,[1] L. Canton,[4] R. Fossión,[5] A. S. Kadyrov,[1] S. Karataglidis,[2,3] J. P. Svenne,[6] and D. van der Knijff[2]

[1]*Department of Physics, Astronomy and Medical Radiation Sciences, Curtin University, GPO Box U1987, Perth 6845, Australia*

[2]*School of Physics, University of Melbourne, Victoria 3010, Australia*

[3]*Department of Physics, University of Johannesburg, P.O. Box 524, Auckland Park, 2006, South Africa*

[4]*Istituto Nazionale di Fisica Nucleare, Sezione di Padova, I-35131, Italy*

[5]*Instituto de Ciencias Nucleares, Universidad Nacional Autónoma de México, 04510, Ciudad de México, Mexico*

[6]*Department of Physics and Astronomy, University of Manitoba and Winnipeg Institute for Theoretical Physics, Winnipeg, Manitoba R3T 2N2, Canada*

(Received 7 May 2016; revised manuscript received 6 July 2016; published 7 September 2016)

What effect do particle-emitting resonances have on the scattering cross section? What physical considerations are necessary when modeling these resonances? These questions are important when theoretically describing scattering experiments with radioactive ion beams which investigate the frontiers of the table of nuclides, far from stability. Herein, a novel method is developed that describes resonant nuclear scattering from which centroids and widths in the compound nucleus are obtained when one of the interacting bodies has particle unstable resonances. The method gives cross sections without unphysical behavior that is found if simple Lorentzian forms are used to describe resonant target states. The resultant cross sections differ significantly from those obtained when the states in the coupled channel calculations are taken to have zero width, and compound-system resonances are better matched to observed values.

DOI: 10.1103/PhysRevC.94.034603

The advent of radioactive ion beams has allowed exploration of nuclei far from the valley of stability, and has led to an immense experimental effort [1–14]. Theoretical studies of these systems are vital for interpretation of the resultant data. Elastic scattering of two nuclei at low energies often gives cross sections displaying resonances associated with properties of the compound system, the analysis of which is appropriately done with a coupled-channel theory in which the low-energy spectra of the nuclei concerned are most relevant in defining the coupling interactions. Usually, however, those states are not considered to be resonances. Herein we present results found using a theory in which those target state resonance properties are taken into account. As detailed below, this requires a mathematically robust, energy-dependent shape to avoid unphysical behaviors in calculated observables, such as vanishing bound states, irregular behavior at the scattering threshold, and with the requirement of causality being restored.

To this end, a multichannel algebraic scattering (MCAS) method [15] is used. MCAS solves coupled-channel Lippmann-Schwinger equations in momentum space using the Hilbert-Schmidt expansion of amplitudes. In this method, two-body nuclear scattering potentials are expanded into a series of sturmians [15–17], and then a corollary between separable scattering potentials and separable T matrices of the Lippmann-Schwinger equation delivers solutions without explicitly solving the integral equations. Scattering potentials used for this investigation have the basic form

$$V_{cc'}(r) = f(r)\{V_0\delta_{cc'} + V_{ll}[\ell\cdot\ell]_{cc'} + V_{ss}[\mathbf{s}\cdot\mathbf{I}]_{cc'}\} + g(r)V_{ls}[\ell\cdot\mathbf{s}]_{cc'}, \quad (1)$$

for each channel (c), where c denotes a unique set of quantum numbers, and with parameters for the central (V_0), orbit-orbit (V_{ll}), spin-spin (V_{ss}), and spin-orbit ($V_{\ell s}$) components. For the functions $f(r)$ and $g(r)$, deformed Woods-Saxon form factors are used:

$$f(r) = \left[1 + e^{\left(\frac{r-R}{a}\right)}\right]^{-1}, \qquad g(r) = \frac{1}{r}\frac{df(r)}{dr}. \quad (2)$$

The radius of the nuclear target is taken to be deformed, and the Woods-Saxon form factors are expanded to the second order in terms of this deformation. To treat the nuclear target as having collective rotor character, deformation is defined in terms of spherical harmonics [18]. Full details can be found in Ref. [19]. In this work we consider only quadrupole deformations.

However, to preclude coupling of the incident nucleon to Pauli-forbidden orbits in the target states, one must also include an orthogonalizing pseudopotential (OPP) [20–24], as has also been used in atomic physics [25,26].

By solving the Lippmann-Schwinger equations in momentum space, one may describe within the same method both the bound (to particle emission) and scattering states of the compound nucleus. Bound states of the compound system can be found by using negative projectile energies, for which all channels are closed. Details are given in Ref. [15]. For positive energies, to systematically identify all resonance structures we use a spectral representation of the S matrix in terms of complex Sturmian eigenvalues [16].

To obtain S and T matrices, sets of Sturmian functions, $\Phi_{c'n}(r)$, and their eigenvalues, η_n, are determined from the coupled-channel interactions, $V_{cc'}(r)$. For practical reasons we choose a set (n) of finite rank, with entries being those having largest magnitudes of η_n. These are used in defining

*paul.fraser@curtin.edu.au

 ©2016 American Physical Society

form factors for the Hilbert-Schmidt expansion of these coupled-channel interactions themselves. The form factors, in momentum space, $\hat{\chi}_{cn}(p)$, are the Fourier-Bessel transforms of

$$\chi_{cn}(r) = \sum_{c'=1} V_{cc'}(r)\Phi_{c'n}(r). \tag{3}$$

Obtaining the Sturmian eigenstates, η_p, requires specification of the Green's function [15]

$$[\mathbf{G}_0]_{nn'} = \mu\left[\sum_{c=1}^{\text{open}} \int_0^\infty \hat{\chi}_{cn}(x)\frac{x^2}{k_c^2 - x^2 + i\varepsilon}\hat{\chi}_{cn'}(x)\,dx - \sum_{c=1}^{\text{closed}} \int_0^\infty \hat{\chi}_{cn}(x)\frac{x^2}{h_c^2 + x^2}\hat{\chi}_{cn'}(x)\,dx\right]. \tag{4}$$

where the wave numbers are

$$k_c = \sqrt{\mu(E - \varepsilon_c)} \quad \text{and} \quad h_c = \sqrt{\mu(\varepsilon_c - E)}, \tag{5}$$

ε_c is the target-state centroid and E is the projectile energy. Typically, the Green's functions are solved by methods of complex analysis.

With these Sturmian form factors,

$$V_{cc'}(p,q) = \sum_n \hat{\chi}_{cn}(p)\,\eta_n^{-1}\,\hat{\chi}_{c'n}(q) \tag{6}$$

and

$$T_{cc'} \propto \sum_{n,n'} \sqrt{k_c}\,\hat{\chi}_{cn}(k_c)([\boldsymbol{\eta} - \mathbf{G}_0]^{-1})_{nn'}\,\hat{\chi}_{c'n'}(k_{c'})\sqrt{k_{c'}}\,. \tag{7}$$

With regards to this investigation, the key feature in the above is the Green's function [15].

The spectrum of the compound system is found from the resolvent in the T matrix, namely $[\boldsymbol{\eta} - \mathbf{G}_0]^{-1}$ where $[\boldsymbol{\eta}\,]_{nn'} = \eta_n\ \delta_{nn'}$. The trajectories of the eigenvalues in the complex-energy plane, in particular in the vicinity of the pole-position $P(1,0)$, can be employed to determine each resonance centroid and width contained in the S matrix, no matter how narrow or large the resonance may be [15]. The bound states of the compound system are defined by the zeros of that matrix determinant when the energy is $E < 0$, all channels then being closed.

Results using the Green's function Eq. (4) (and from those later given) are shown in Figs. 1 and 2 using potential strengths and deformations as per Table I. Fig. 1 presents spectra of ^{9}Be as an $n + {}^8$Be cluster and Fig. 2 shows a set of total elastic and reaction cross sections in the energy range to just over 5 MeV. ^{8}Be was treated as a rotor with quadrupole deformation and three states of it, $0^+_{g.s.}$, 2^+_1, and 4^+_1, were used in the coupling. In Fig. 1, the spectrum for ^{9}Be found using Green's functions as per Eq. (4) is shown in the column furthest right. For comparison, the experimental spectrum [27], is shown on the far left. Figure 2 displays the cross sections found from the same calculation (and others discussed later) whose spectrum is shown in Fig. 1. The results are identified by the same notation. In this case, where Eq. (4) is used, the reaction cross section only becomes nonzero above the energy of the first target state, which is at 3.41 MeV (laboratory frame), as necessary.

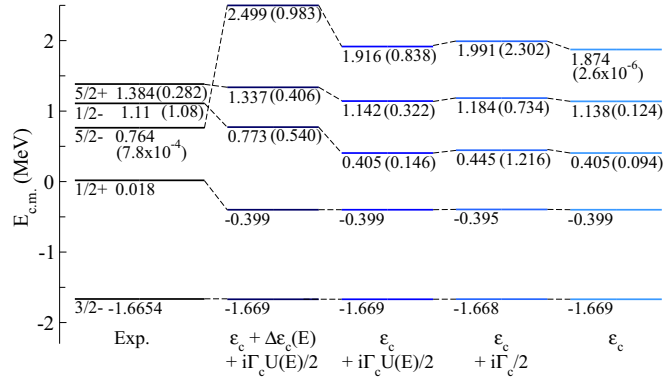

FIG. 1. Experimental spectrum of ^{9}Be compared with MCAS calculations with target states defined as per labels (see text). Unbracketed numbers are excitation energies, bracketed numbers are widths, all in MeV.

However, in the low-energy and low-mass regime where compound-system resonances are important, it is appropriate to take particle instability of target states into account by modifying the Green's functions. In its most basic form [28], this is done by adding a complex component to the target-state energy. That is, the description of the target state energy

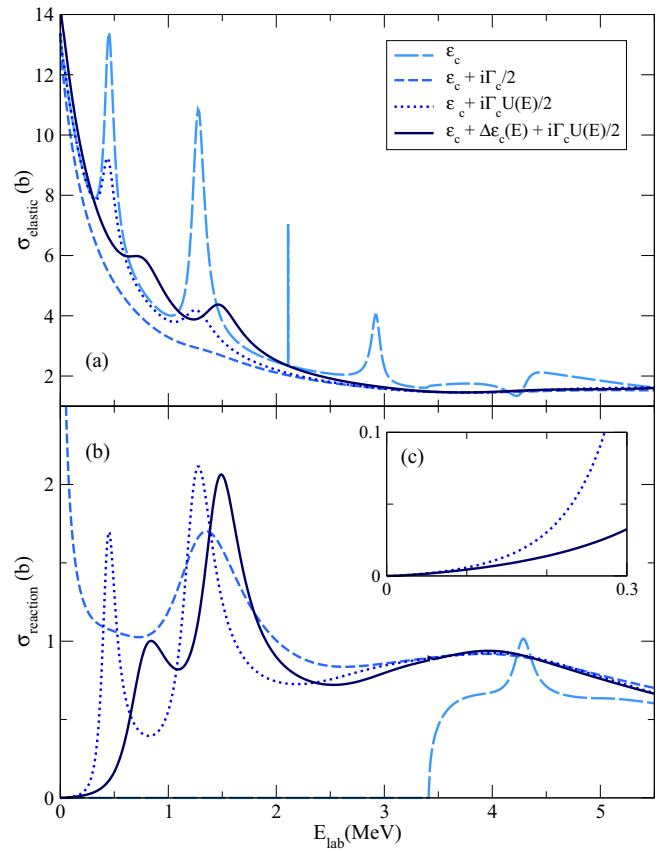

FIG. 2. Calculated $n + {}^8$Be elastic scattering (a) and reaction (b) cross sections. Inset (c) shows threshold behavior of the reaction cross sections.

TABLE I. Parameter values defining the $n + {}^8$Be interaction. $\lambda^{(\mathrm{OPP})}$ are blocking strengths of occupied shells, in MeV. ε_c and Γ_c data from Ref. [27].

		Odd parity		Even parity
V_0 (MeV)		-33.600		-42.975
V_{ll} (MeV)		4.50		0.75
V_{ls} (MeV)		13.40		7.40
V_{ss} (MeV)		4.00		0.00
R_0		a_0		β_2
3.0 fm		0.65 fm		0.50
Target state	ε_c	Γ_c	$\lambda^{(\mathrm{OPP})}\,1s_{1/2}$	$\lambda^{(\mathrm{OPP})}\,1p_{3/2}$
0^+	0.00	5.57 eV[a]	10^6	0.00
2^+	3.03	1.50	10^6	3.50
4^+	11.35	3.50	10^3	0.00

[a]Treated as 0 MeV in calculation.

becomes

$$\varepsilon_c + i\frac{\Gamma_c}{2}, \tag{8}$$

and the Green's functions thus become

$$[\mathbf{G}_0]_{nn'} = \mu\left[\sum_{c=1}^{\text{open}}\int_0^\infty \hat{\chi}_{cn}(x)\frac{x^2\left[k_c^2 - x^2 - \frac{i\mu\Gamma_c}{2}\right]}{\left[k_c^2 - x^2\right]^2 + \frac{\mu^2\Gamma_c{}^2}{4}}\hat{\chi}_{cn'}(x)\,dx - \sum_{c=1}^{\text{closed}}\int_0^\infty \hat{\chi}_{cn}(x)\frac{x^2\left[h_c^2 + x^2 + \frac{i\mu\Gamma_c}{2}\right]}{\left[h_c^2 + x^2\right]^2 + \frac{\mu^2\Gamma_c{}^2}{4}}\hat{\chi}_{cn'}(x)\,dx\right]. \tag{9}$$

This equation has no poles on the real axis, and integration may proceed normally [28]. The spectrum in Fig. 1 identified by the complex energy $\epsilon_c + i\frac{\Gamma}{2}$ resulted when using the same interaction as before but with the 2^+ and 4^+ states of ^{8}Be having their known particle-emission widths [27].

Cross sections are calculated using the S matrix, which has the general form

$$S_{cc'} = \delta_{cc'} - i^{l_{c'}-l_c+1}\pi\mu\sum_{n,n'=1}^{N}\sqrt{k_c}\hat{\chi}_{cn}(k_c) \times ([\boldsymbol{\eta} - \mathbf{G}_0]^{-1})_{nn'}\hat{\chi}_{c'n'}(k_{c'})\sqrt{k_{c'}}, \tag{10}$$

where $\boldsymbol{\eta}$ is an array of Sturmian eigenvalues. $\mathbf{G}_0$ is the Green's function defined by Eq. (4) in the case where no target state widths are considered, and by Eq. (9) in the case where states are described as per Eq. (8). As the systems considered herein do not have particle emission widths in their ground states, the Sturmians "in the elastic channel" $\hat{\chi}_{1n}(k_1)$ and $\hat{\chi}_{1n}(k_1)$ will not be different from cases where no target-state widths are considered. However, S matrices and thus cross sections will still be altered by the inclusion of particle-emission widths through the channels of $([\boldsymbol{\eta} - \mathbf{G}_0]^{-1})_{nn'}$ not involving the target ground state. The cross sections that result from using complex energies for the 2_1^+ and 4_1^+ states in ^{8}Be, are shown in Fig. 2, identified by the notation $\epsilon_c + i\frac{\Gamma}{2}$.

Of note, with particle-emission considered, the reaction cross section is nonzero from zero projectile energy upwards, due to loss of flux from target decay. However, its asymptotic behavior at low projectile energies is unphysical, and is due to the Lorentzian form that implicitly defines the target states in Eq. (9) being nonzero at and below the scattering threshold, as also observed in a technical note, Ref. [29]. This also affects the energy of bound states, causing some to become spuriously unstable.

To overcome this nonphysical behavior, a scaling factor is applied to target-state widths, such that the target states are now described as

$$\varepsilon_c + i\frac{U(E)\Gamma_c}{2}, \tag{11}$$

which changes the Green's functions of Eq. (9) by multiplication of Γ_c in both integrals by $U(E)$. The minimum conditions placed on the scaling function are

$$U(E) = 0 \quad \text{at } E \leqslant 0,$$
$$U(E) = 1 \quad \text{at } E = \varepsilon_c,$$
$$U(E) \to 0 \quad \text{as } E \to \infty.$$

In addition, to fully eliminate asymptotic behavior in the reaction cross sections, it is required that

$$\frac{dU(E)}{dE} \to 0 \quad \text{as } E \to +0.$$

See Ref. [29] for an example in which a scaling function was investigated where the last condition was not met (and where causality correction, discussed below, was not addressed.)

The concept of energy dependent widths goes back to Wigner [30], and is widely used in nuclear cross section estimates [31]. Typically, the low-energy dependence of such scaled resonances are ruled by the centrifugal (and eventually Coulomb) barrier. The probability of formation of a resonance is modulated at low energies by these "penetration" factors. It is these factors which lead to the requirement on the scaling functions that they and their derivatives are vanishing at the scattering threshold.

However, the introduction of energy-dependent widths necessitates an energy-dependent addition to the target-state centroid, transforming the energy of the state to

$$\varepsilon_c + \Delta\varepsilon_c(E) + i\frac{\Gamma_c U(E)}{2}. \tag{12}$$

This is because the Green's functions define the Sturmian eigenvalues of the expansion of the potential. Thus, making the prescription of the target states complex effectively makes the potential an optical potential. As detailed in Refs. [32,33], energy-dependent complex components in optical potentials lead to a wave equation that violates causality unless the potential is restricted by the addition of a dispersion relation to the real part of the potential. These concepts have been used in phenomenological optical models in, for example, Refs. [34,35].

Here, the dispersion relation is an energy-dependent adjustment of the target-state centroid energy, $\Delta\varepsilon_c(E)$, given by the

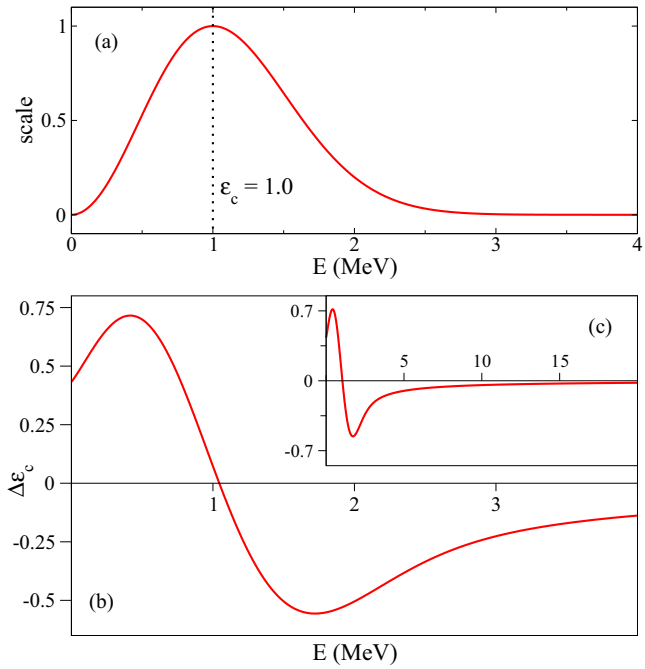

FIG. 3. (a) Scaling function $U(E)$ of Eq. (15) for $q = 1$, and $Z = 2$ with $\varepsilon_c = 1$. (b) Numerically evaluated $\Delta\varepsilon_c(E)$ with $U(E)$ having parameters as above and $\Gamma_c = 2$ MeV. (c) Inset showing approach to -0 as projectile energy increases.

principal part integral

$$\Delta\varepsilon_c(E) = \frac{\Gamma_c}{2}\frac{1}{\pi} P \int_0^\infty \frac{U(E')}{E' - E} dE' . \tag{13}$$

This manifests in Eq. (9) [with Γ multiplied by $U(E)$] as wave numbers with the form

$$k_c = \sqrt{\mu[E - \varepsilon_c - \Delta\varepsilon_c(E)]},$$
$$h_c = \sqrt{\mu[\varepsilon_c + \Delta\varepsilon_c(E) - E]}. \tag{14}$$

Many nuclear targets have a ground state with no particle-emission width, and when considering the channels involving those ground states, the wave numbers have the form of Eq. (5) rather than Eq. (14), and the Green's function of Eq. (4) applies rather than Eq. (9) [modified by $U(E)$ and $\Delta\varepsilon_c(E)$].

One candidate for an energy-dependent target-state width scaling is based upon a Wigner distribution [36], modified to meet the necessary conditions

$$U(E) = e^q \left(\frac{E}{\varepsilon_c}\right)^Z e^{-q(E/\varepsilon_c)^Z} H(E), \tag{15}$$

where q and Z are positive parameters. The Heaviside function ensures proper bound-state properties. Without it the Green's function is complex for negative E. The upper panel of Fig. 3 shows the scaling function of Eq. (15) for $q = 1$, and $Z = 2$. The lower panel shows the integrated result of Eq. (13) with $\varepsilon_c = 1$ MeV and $\Gamma_c = 2$ MeV.

At projectile energies below that of a resonant target state's actual centroid, the effect of reducing the width of that state increases the centroid used for purposes of defining the wave number. Conversely, at projectile energies above the actual centroid, the reduction in target state width decreases the centroid used. The transition from positive to negative centroid correction occurs at $E > \varepsilon_c$ for these values of q and Z, which is caused by the exponential suppression of the scaling function $U(E)$ at energies larger than E. As projectile energy tends to infinity, the centroid correction tends to $+0$.

Column 2 of Fig. 1 shows the resonances and bound states of an MCAS calculation with resonant states defined as per Eq. (12), using the Green's function defined accordingly. The calculation used the same potential as all the others, and in fact the parameters were tuned for this case. The appropriately labeled curves in Fig. 2 show the resultant elastic and reaction cross sections. Column 3 of Fig. 1 and the matching curves of Fig. 2 show the results of the energy-dependent scaling of widths but neglecting the causality correction to the centroid energy.

It is seen from differences between columns 2 and 5 of Fig. 1 that consideration of nuclear instability in scattering calculations has nontrivial impact upon compound-state centroids, affecting how scattering potentials must be defined to match experiment. The differences between column 2 and 3 show that the causality correction accounts for a significant part of this variation. The result of the full physical description of target states (column 2) gives the best centroid values for the $\frac{1}{2}^-$ and $\frac{5}{2}^+$ resonances, the features that dominate the calculated cross sections.

The $\frac{1}{2}^-$ resonance is only known to decay by neutron emission, and the $\frac{5}{2}^+$ resonance by neutron and γ emission [27], and so this MCAS calculation considers all important components of the resonances' widths. The calculation with no consideration of ^{8}Be decay widths (column 5) leads a width for the $\frac{1}{2}^-$ state that is only 9% of that observed experimentally, where the calculation with target-state width scaling and causality correction (column 2) gives a result that is 50% of the known value. The calculation in which decay widths are included but not scaled (column 4) produces 112% of the known value, but as with column 3, the calculated result is unphysical as previously discussed. Regarding the $\frac{5}{2}^+$ resonance, the width result in column 5 is 44% of the experimental value, while that of column 2 is 144%, a slightly better ratio, and that of column 4 is a large overestimation at 260%. The centroid of the $\frac{5}{2}^-$ resonance is poorly recreated in all calculations, and concordantly the widths are over- or underestimated in all cases by orders of magnitude. Thus, certainly in the case of the $\frac{1}{2}^-$ resonance, and arguably that of the $\frac{5}{2}^+$ resonance, consideration of particle emission from target states is seen to be a necessary ingredient in better describing scattering involving loosely bound nuclei. Further investigation of scaling factor forms may yield yet better descriptions of compound-system resonance shapes.

The appropriately labeled curves in Fig. 2 show cross sections resulting from defining target states as per Eq. (12), and with target state width scaling but neglecting the causality correction. Again the reaction cross section is nonzero from zero projectile energy upwards due to flux loss, but it is observed that the scaling factor successfully eliminates the erroneous asymptotic rise in the reaction cross section near

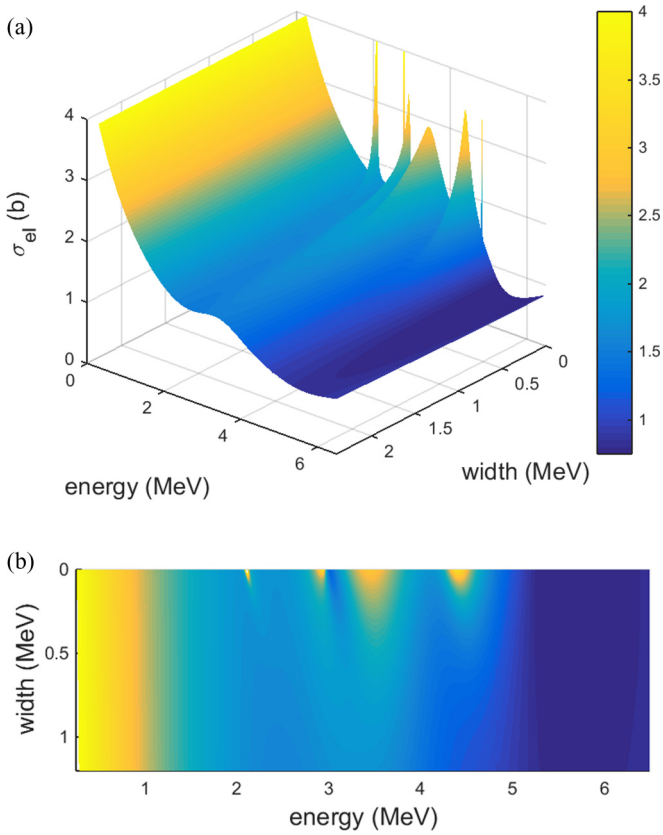

FIG. 4. (a) $n + {}^{12}$C elastic scattering cross section with *gedanken* particle-emission widths, Γ_c, of ^{12}C 2_1^+ and 0_2^+ states as per the axis. E is the projectile energy. (b) Contour map detail of the top panel. Target states are as per the right of Eq. (12), with $q = 1$, $Z = 2$ in Eq. (15).

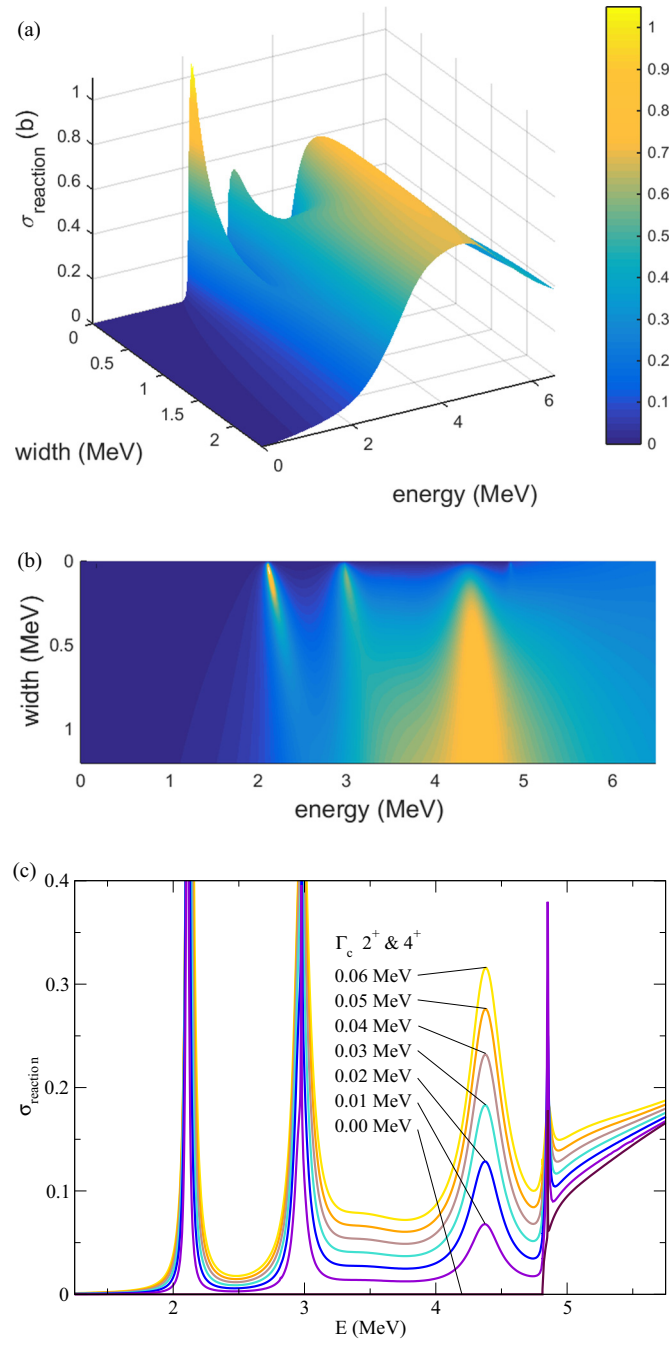

FIG. 5. (a) $n + {}^{12}$C reaction cross section with *gedanken* particle-emission widths, Γ_c, of ^{12}C 2_1^+ and 0_2^+ states as per the axis. E is the projectile energy. (b) Contour map detail of the top panel. Target states are as per the right of Eq. (12), with $q = 1$, $Z = 2$ in Eq. (15) (c) Detail, showing behavior of reaction cross section for small widths.

the threshold. This is highlighted by the inset panel. Causality restoration, by altering centroids, affects the shape of the cross sections, with consequences for scattering-potential parametrization.

To further illustrate the effect of the Green's functions of Eq. (9) modified with $U(E)$ and $\Delta\varepsilon_c(E)$, we examine a *gedanken* case of the scattering of low-energy neutrons from ^{12}C, with coupling of the neutron to the 0_1^+, 2_1^+, and 0_2^+ states of ^{12}C. A range of artificial particle-emission widths are assigned to the 2_1^+ and 0_2^+ states of the target, with the resulting elastic-scattering and reaction cross sections shown in Figs. 4 and 5, respectively. Note that the width scaling factor, Eq. (15), tends to zero as ε_c tends to zero, meaning that within this formalism ground state widths cannot be considered. Thus, ground state widths are set to zero and the principle-parts method of solving the Green's functions of Eq. (4) is retained for this channel.

Figure 4 shows that, while the inclusion of target state widths has minimal impact upon the scattering background, with increasing target-state widths, compound-system resonances are reduced in amplitude and increased in width. With increasing target-state widths, narrow resonances are subsumed into the scattering background. The wider compound-state resonances persist to greater widths. Note that, even when not discernible from the scattering background, the method of obtaining resonances outlined above still identifies them.

The contour map view in the second panel of Fig. 5 shows that when target-state widths equal 0 MeV, the reaction cross section only becomes nonzero above the energy of the first target state, at 4.81 MeV (laboratory frame), as is necessary. When target-state widths are increased, the reaction cross section becomes non-zero for all projectile energies greater

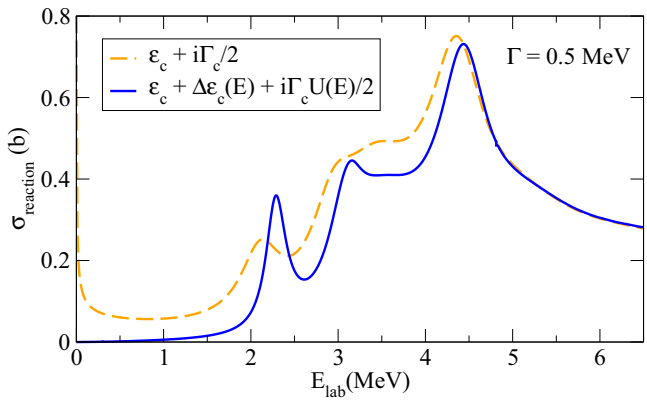

FIG. 6. Calculated $n + {}^{12}\mathrm{C}$ reaction cross for $\Gamma_c = 0.5\,\mathrm{MeV}$.

than the scattering threshold, as particle decay leads to flux loss. As target widths increase from zero, compound-system resonances immediately appear and dominate this region below the first target state energy. The third panel presents several reaction cross sections at small Γ_c to show their behavior in more detail.

The second panel further shows that as widths increase, these resonances rapidly become subsumed into the scattering background. No unphysical asymptotic behavior is observed at projectile energies near the scattering threshold.

To further examine behavior of the reaction cross section near the scattering threshold, Fig. 6 shows the case of the $^{12}\mathrm{C}$ 2_1^+ and 0_2^+ states each having a width of 0.5 MeV. The two results shown used target states defined as per Eqs. (8) and (12) respectively. As in the $^{9}\mathrm{Be}$ investigation, the former has erroneous asymptotic behaviour as $E \to +0$, which is eliminated in the latter.

In conclusion, a method of accounting for states that are particle unstable in nuclei undergoing low-energy resonant scattering is developed, which is free of unphysical behavior at the scattering threshold and conserves causality. This is performed by choosing an appropriate target-state resonance shape, modifying a Lorentzian by use of widths dependent on projectile energy, with a correction to target-state centroid energy. Resultant scattering cross sections are markedly different from those found when particle instability is not considered. Compound-system resonances decrease in magnitude and increase in width, with otherwise narrow resonances becoming obscured into the scattering background. This was shown to improve agreement between calculated and observed widths of such resonances. When using parameter-driven scattering potentials, the effects of the target-state resonance shape—and in the case energy-dependent modified Lorentzians, the centroid correction—are nontrivial in defining the potential. Compound spectra associated with, and scattering cross sections from, weakly bound radioactive ion beams with light-mass targets should be influenced by such considerations as these.

This work is supported by the Australian Research Council, National Research Foundation of South Africa, and U.S. National Science Foundation under Grant No. PHY-1415656.

[1] C. A. Bertulani and G. Baur, Phys. Rep. **163**, 299 (1988).
[2] N. Orr, J. Phys. G **38**, 020301 (2011).
[3] M. Huyse and R. Raabe, J. Phys. G **38**, 024001 (2011).
[4] J. R. Beene *et al.*, J. Phys. G **38**, 024002 (2011).
[5] G. C. Ball *et al.*, J. Phys. G **38**, 024003 (2011).
[6] A. Navin *et al.*, J. Phys. G **38**, 024004 (2011).
[7] P. V. Duppen and K. Riisager, J. Phys. G **38**, 024005 (2011).
[8] A. B. Balantekin *et al.*, Mod. Phys. Lett. A **29**, 1430010 (2014).
[9] B. B. Back *et al.*, AIP Adv. **4**, 041005 (2014).
[10] F. D. Becchetti *et al.*, Nucl. Instrum. Methods Phys. Res., Sect. A **505**, 377 (2003).
[11] A. Lepine-Szily *et al.*, Nucl. Phys. A **834**, 491c (2010).
[12] H. Okuno, N. Fukunishi, and O. Kamigaito, Prog. Theor. Exp. Phys. (2012) 03C002.
[13] Z. Sun *et al.*, Nucl. Instrum. Methods Phys. Res., Sect. A **503**, 496 (2003).
[14] R. Rafiei *et al.*, Nucl. Instrum. Methods Phys. Res., Sect. A **631**, 12 (2011).
[15] K. Amos *et al.*, Nucl. Phys. A **728**, 65 (2003).
[16] S. Weinberg, *Lectures on Particles and Field Theory* (Prentice-Hall, Englewood Cliffs, NJ, 1965).
[17] G. H. Rawitscher and L. Canton, Phys. Rev. C **44**, 60 (1991).
[18] T. Tamura, Rev. Mod. Phys. **37**, 679 (1965).
[19] P. R. Fraser, L. Canton, K. Amos, S. Karataglidis, J. P. Svenne, and D. van der Knijff, Phys. Rev. C **90**, 024616 (2014).
[20] V. M. Krasnopolsky and V. I. Kukulin, Yad. Fiz. **20**, 883 (1974) [Sov. J. Nucl. Phys. **20**, 470 (1975)].
[21] V. Kukulin and V. Pomerantsev, Ann. Phys. (NY) **111**, 330 (1978).
[22] S. Saito, Prog. Theor. Phys. **41**, 705 (1969).
[23] L. Canton, G. Pisent, J. P. Svenne, D. van der Knijff, K. Amos, and S. Karataglidis, Phys. Rev. Lett. **94**, 122503 (2005).
[24] K. Amos *et al.*, Nucl. Phys. A **912**, 7 (2013).
[25] J. Mitroy and G. G. Ryzhikh, Comput. Phys. Commun. **123**, 103 (1999).
[26] I. A. Ivanov, M. W. J. Bromley, and J. Mitroy, Comput. Phys. Commun. **152**, 9 (2003).
[27] D. R. Tilley *et al.*, Nucl. Phys. A **745**, 155 (2004).
[28] P. Fraser, K. Amos, L. Canton, G. Pisent, S. Karataglidis, J. P. Svenne, and D. van der Knijff, Phys. Rev. Lett. **101**, 242501 (2008).
[29] L. Canton, P. R. Fraser, J. P. Svenne, K. Amos, S. Karataglidis, and D. van der Knijff, Phys. Rev. C **83**, 047603 (2011).
[30] T. Teichmann and E. Wigner, Phys. Rev. **87**, 123 (1952).
[31] C. Broggini, L. Canton, G. Fiorentini, and F. L. Villante, J. Cosmol. Astropart. Phys. 06 (2012) 030.
[32] J. M. Cornwall and M. A. Ruderman, Phys. Rev. **128**, 1474 (1962).
[33] C. Mahaux *et al.*, Nucl. Phys. A **449**, 354 (1986).
[34] C. Mahaux *et al.*, Nucl. Phys. A **456**, 134 (1986).
[35] G. Cattapan, L. Canton, and G. Pisent, Phys. Rev. C **43**, 1395 (1991).
[36] M. Mehta, *Random Matrices* (Academic, New York, 1991).